Atmos. Chem. Phys., 14, 1353–1369, 2014
www.atmos-chem-phys.net/14/1353/2014/
doi:10.5194/acp-14-1353-2014

Atmospheric Chemistry and Physics Open Access

Constraints on ship NO_x emissions in Europe using GEOS-Chem and OMI satellite NO_2 observations

G. C. M. Vinken[1], K. F. Boersma[2,3], A. van Donkelaar[4], and L. Zhang[5]

[1]Department of Applied Physics, Eindhoven University of Technology, Eindhoven, the Netherlands
[2]Department of Meteorology and Air Quality, Wageningen University, Wageningen, the Netherlands
[3]Climate Observations Department, Royal Netherlands Meteorological Institute, De Bilt, the Netherlands
[4]Department of Physics and Atmospheric Science, Dalhousie University, Halifax, Nova Scotia, Canada
[5]Department of Atmospheric and Oceanic Sciences & Laboratory for Climate and Ocean-Atmosphere Studies, School of Physics, Peking University, Beijing 100871, China

Correspondence to: G. C. M. Vinken (g.c.m.vinken@tue.nl)

Received: 7 June 2013 – Published in Atmos. Chem. Phys. Discuss.: 23 July 2013
Revised: 18 December 2013 – Accepted: 20 December 2013 – Published: 5 February 2014

Abstract. We present a top-down ship NO_x emission inventory for the Baltic Sea, the North Sea, the Bay of Biscay and the Mediterranean Sea based on satellite-observed tropospheric NO_2 columns of the Ozone Monitoring Instrument (OMI) for 2005–2006. We improved the representation of ship emissions in the GEOS-Chem chemistry transport model, and compared simulated NO_2 columns to consistent satellite observations. Relative differences between simulated and observed NO_2 columns have been used to constrain ship emissions in four European seas (the Baltic Sea, the North Sea, the Bay of Biscay and the Mediterranean Sea) using a mass-balance approach, and accounting for non-linear sensitivities to changing emissions in both model and satellite retrieval. These constraints are applied to 39 % of total top-down European ship NO_x emissions, which amount to 0.96 Tg N for 2005, and 1.0 Tg N for 2006 (11–15 % lower than the bottom-up EMEP ship emission inventory). Our results indicate that EMEP emissions in the Mediterranean Sea are too high (by 60 %) and misplaced by up to 150 km, which can have important consequences for local air quality simulations. In the North Sea ship track, our top-down emissions amount to 0.05 Tg N for 2005 (35 % lower than EMEP). Increased top-down emissions were found for the Baltic Sea and the Bay of Biscay ship tracks, with totals in these tracks of 0.05 Tg N (131 % higher than EMEP) and 0.08 Tg N for 2005 (128 % higher than EMEP), respectively. Our study explicitly accounts for the (non-linear) sensitivity of satellite retrievals to changes in the a priori NO_2 profiles, as satellite observations are never fully independent of model information (i.e. assumptions on vertical NO_2 profiles). Our study provides for the first time a space-based, top-down ship NO_x emission inventory, and can serve as a framework for future studies to constrain ship emissions using satellite NO_2 observations in other seas.

1 Introduction

Strong emissions of gases and particulate matter by ships affect the composition of the marine boundary layer, with important consequences for climate change, air quality and public health. Because hardly any regulations for the maritime sector exist in international waters, ships are still allowed to burn marine heavy fuel, resulting in substantial emissions of black carbon (BC), sulfur dioxide (SO_2), nitrogen oxides ($NO_x = NO + NO_2$), and volatile organic compounds (VOCs) (e.g. Eyring et al., 2010). NO_x and SO_2 emissions from ships are relatively high compared to emissions from other transport sectors because marine heavy fuel is high in sulfur content and is combusted at high temperatures without reduction technologies (Eyring et al., 2005). Recently, new legislation has been proposed that sets limits on technology used in new ships to reduce sulfur and nitrogen oxide emissions in so-called sulfur emission control areas (SECAs) and NO_x emissions control areas (NECAs). In Europe, SECAs have been in effect since 2006 and 2007 for the North Sea

and the Baltic Sea, respectively, and a NECA is planned for the Baltic Sea for 2016. The North American coastal waters are designated as both a SECA and NECA since 2012 (IMO, 2009). Stringent emission limits for ships in these seas will be enforced in several steps, but the International Maritime Organization (IMO) is currently considering delaying the implementation of tighter limits in NECAs.

NO_x emissions lead to O_3 and particulate matter formation, detrimental to air quality in the densely populated coastal regions close to ship lanes. Furthermore, O_3 influences the hydroxyl radical (OH) concentrations that determine the lifetime of methane (CH_4) (Lawrence and Crutzen, 1999), thereby influencing its global radiative forcing (IPCC, 2007). Sulfate (SO_4^{2-}) formed by oxidation of sulfur dioxide (SO_2) is the dominant aerosol emitted from ships and has a negative radiative forcing (due to its efficient reflection of sunlight). Aerosols originating from ships can also have an indirect (negative) effect on radiative forcing by altering the properties of clouds (e.g. Schreier et al., 2007; Lauer et al., 2007). Because of their important effect on both air quality and climate, ship emissions have received increasing attention over the past years. Previous studies (e.g. Corbett et al., 2007; Eyring et al., 2010; Paxian et al., 2010) proposed that global ship NO_x emissions amount to 3.0–10.4 Tg N per year (15–35 % of global anthropogenic NO_x emissions). However, as individual measurements of ship emissions are sparse, and knowledge of activity, technology and global fleet is limited, these bottom-up inventories suffer from large uncertainties, making it difficult to assess the efficacy of reducing ship emissions in order to mitigate the effects of air pollution and climate change.

The magnitude and geographic location of ship NO_x emissions can be constrained by using high-spatial-resolution satellite observations of NO_2 columns. Previous studies have demonstrated this concept, where satellite-observed NO_2 columns, in combination with simulations from a chemistry transport model (CTM), were used to constrain NO_x emissions. For example, Martin et al. (2003) used observations from the Global Ozone Monitoring Experiment (GOME) instrument to scale global NO_x emissions in the GEOS-Chem CTM. Different instruments have since then been used to constrain various source categories: anthropogenic emissions (e.g. Martin et al., 2006), soil NO_x (e.g. Jaeglé et al., 2005) and lightning NO_x (e.g. Boersma et al., 2005). Recently, Wang et al. (2012) used high-resolution NO_2 columns from the Ozone Monitoring Instrument (OMI) to detect newly built power plants in China.

Satellite observations have also provided information on ship pollution. Beirle et al. (2004) used GOME measurements of tropospheric NO_2 columns to estimate emissions in the ship lane from Sri Lanka to Indonesia. Several ship tracks have been identified in global maps of satellite-observed NO_2 columns from the SCanning Imaging Absorption spectroMeter for Atmospheric CartograpHY (SCIAMACHY) and compared to an emission inventory by Richter et al. (2004). Marmer et al. (2009) took advantage of the higher spatial and temporal resolution of OMI NO_2 observations of the ship track in the Mediterranean Sea to assess several emissions inventories. A trend in NO_2 columns over four ship tracks in Europe and Asia, following the rhythm of global economic activity, was shown by de Ruyter de Wildt et al. (2012) using GOME, SCIAMACHY, OMI and GOME-2 observations. Franke et al. (2009) used a combination of observed NO_2 columns of SCIAMACHY, GOME and GOME-2 instruments and modelled columns using the ECHAM5/MESSy1 CTM to evaluate ship NO_x emissions in the ship track from Sri Lanka to Indonesia. They concluded that their modelled NO_2 columns were in good agreement with observed columns for 2002–2007. However, as with most CTMs, their model neglected the in-plume chemistry of ship emissions by instantly diluting the emissions over the model grid cell. This results in an overestimation of modelled NO_x concentrations (e.g. Kasibhatla et al., 2000; Davis et al., 2001; Vinken et al., 2011) and therefore in too low ship NO_x emissions estimates. Various methods have been proposed in the literature to account for the non-linear chemistry during the first stages of ship plume expansion (for a review, see Paoli et al., 2011). Here we use our recently developed method using a plume-in-grid approach (Vinken et al., 2011) that accounts for the non-linear in-plume chemistry in the GEOS-Chem global 3-D CTM. Compared to instant dilution of ship emissions, this method leads to lower (simulated) background NO_x concentrations over the North Atlantic Ocean by up to 60 %.

In this study we focus on providing top-down constraints on ship NO_x emissions by comparing modelled and satellite-observed NO_2 columns for four major ship routes in Europe (the Mediterranean Sea, the Bay of Biscay, the Baltic Sea and the North Sea). This is the first time that NO_2 pollution has been evaluated using satellite measurements over the Bay of Biscay, the Baltic Sea and the North Sea. These observed columns are compared to NO_2 columns simulated with the nested version of the GEOS-Chem CTM. The high-resolution ($1/2^\circ \times 2/3^\circ$) of the nested version of GEOS-Chem is capable of resolving major ship tracks in Europe, and improves the localization of emissions. We run the European nested version of GEOS-Chem at a $1/2^\circ \times 2/3^\circ$ resolution for 2005–2006 using the plume-in-grid treatment of ship NO_x emissions introduced in Vinken et al. (2011). Using the combination of the high-resolution modelled columns and OMI-observed columns, we present for the first time space-based, seasonal and annual constraints on ship NO_x emissions in four major European ship routes for 2005–2006.

Table 1. Overview of total European 2005–2006 NO_x emissions used in this study ($Tg\,N\,yr^{-1}$)[a].

Type	Total 2005	Total 2006	Inventory/Source
Anthropogenic	5.4	5.3	EMEP Vestreng et al. (2007)
Aircraft	0.1	0.1	Baughcum et al. (1996)
Biofuel burning	0.2	0.2	Yevich and Logan (2003)
Fertilizer use	0.3	0.3	Wang et al. (1998)
Ship	1.1	1.2	EMEP & AMVER-ICOADS[b] Vestreng et al. (2007); Wang et al. (2008)
Biomass burning	0.1	0.1	van der Werf et al. (2006)
Lightning	0.5	0.5	Sauvage et al. (2007)
Soil	0.5	0.5	Wang et al. (1998)
Total	8.3	8.3	

[a] $1\,Tg\,N = 3.29\,Tg\,NO_2$.
[b] Combination of both inventories; see Sect. 3.1 for further details.

2 Simulations and satellite observations of tropospheric NO_2 columns

2.1 GEOS-Chem model

Here we use the GEOS-Chem (v8-03-02, http://geos-chem.org) chemistry transport model to simulate tropospheric NO_2 columns over Europe for 2005–2006. The nested-grid version of GEOS-Chem (Wang et al., 2004; Chen et al., 2009; Zhang et al., 2012) is operated at $1/2° \times 2/3°$ resolution with 47 vertical layers, and a transport and chemistry time step of 10 and 20 min, respectively. The boundary conditions are updated every 3 h using global simulations from the $2° \times 2.5°$ parent model (one-way nesting). Both the nested and global simulations are driven by GEOS-5 assimilated meteorological observations from the NASA Global Modeling and Assimilation Office (GMAO). The nested-grid domain extends from 30 to 70° N and 30° W to 50° E. The lowermost layer of the model has an approximate depth of 120 m and the vertical extent of the model is 80 km. GEOS-Chem has a detailed simulation of ozone–NO_x–hydrocarbon–aerosol chemistry, as recently described and discussed by Mao et al. (2010) and Lin et al. (2012). The reactive uptake coefficient $\gamma_{N_2O_5}$ for N_2O_5 on aerosols is from Macintyre and Evans (2010), with a resulting annual mean value for 2005 of $\gamma_{N_2O_5}$ in surface air over our domain of 0.004, at the high end of recently measured values (0.0005–0.006; Brown et al., 2009; Bertram et al., 2009). We performed a spin-up of 1 yr (2004) and simulations for 2005–2006. Daily simulated tropospheric NO_2 columns corresponding to the satellite overpass time (between 13:00 and 15:00 LT) were averaged. To ensure consistency with the satellite observations, only days with valid satellite observations (see next section) were included.

Global anthropogenic emissions are from the Emission Database for Global Atmospheric Research (Olivier and Berdowski, 2001). Over Europe these are replaced with the Monitoring and Evaluation of the Long-range Transmission of Air Pollutants in Europe (EMEP) inventory (Vestreng et al., 2007). We replaced ship emissions (NO_x, SO_2 and CO) from the EMEP inventory with a combination of the EMEP and (global) AMVER-ICOADS (Wang et al., 2008) inventories, as emissions were misplaced in the EMEP inventory (see discussion in Sect. 3.1). NO_x emissions from soils are included based on the parametrization of Yienger and Levy II (1995) and Wang et al. (1998). Furthermore, lightning (Sauvage et al., 2007), biomass burning (van der Werf et al., 2006), biofuel (Yevich and Logan, 2003) and aircraft (Baughcum et al., 1996) NO_x emissions are included in the model. An overview of the total NO_x emissions over Europe for 2005–2006 used in this study is given in Table 1. Anthropogenic sources ($7.2\,Tg\,N\,yr^{-1}$; including aircraft, biofuel, fertilizer use and ships) account for 87 % of the total NO_x emissions in 2005. Natural emissions (biomass burning, lightning and soil) peak in summer, accounting for 25 % of total European NO_x emissions in July and August 2005.

We use the plume-in-grid approach developed by Vinken et al. (2011) to take into account non-linear chemistry occurring in ship plumes immediately after emission. In that approach a Gaussian plume model with chemistry has been used to construct a look-up table (LUT) that contains the fraction of NO_x remaining and (net) O_3 produced in 5 h of plume expansion after emission as a function of several environmental parameters. Here we extend this method in two ways. First, we limit the chemical aging time in the expanding plume model to 2.5 h, as the plume typically grows to the size of the model grid cell ($1/2° \times 2/3°$) within this time. We store the fraction of NO_x remaining and (net) O_3 produced after 2.5 h of plume expansion in a LUT and multiply GEOS-Chem NO_x emissions with this fraction of NO_x remaining upon release in the model grid cell. The resulting NO_x concentrations in (GEOS-Chem) grid cells with ship emissions can be considered as background concentrations, i.e. representative for NO_x concentrations after a ship passed by 2.5 h earlier. Because we will compare the simulated columns with satellite-observed NO_2 columns, which also include

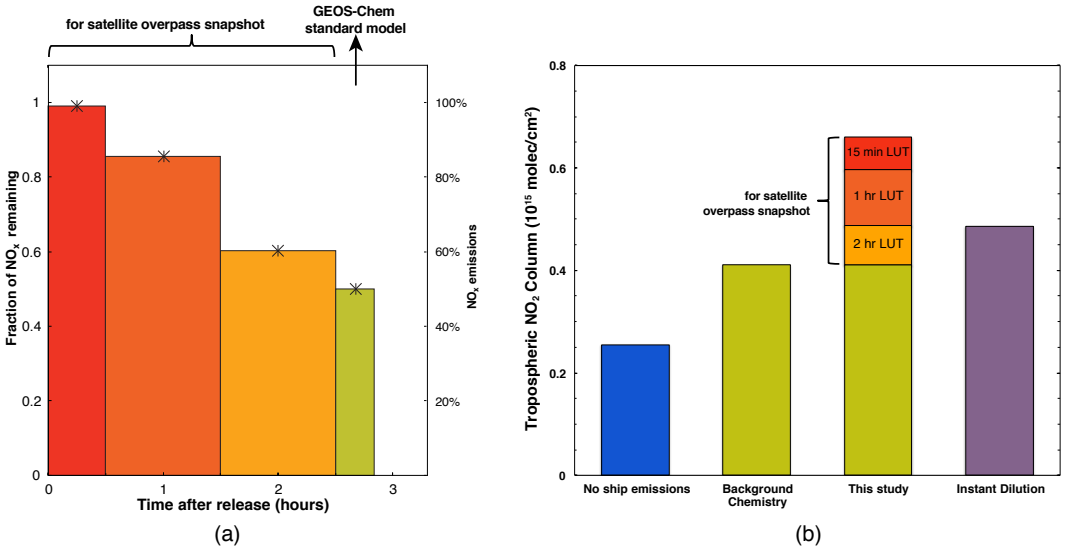

Fig. 1. **(a)** Fraction of NO_x remaining as a function of time passed since emission. Fractions have been calculated by the PARANOX Gaussian plume model for a grid cell in the Bay of Biscay (averaged between 13:00 and 15:00 LT) and include the effects of plume expansion and chemistry (Vinken et al., 2011). Resulting emissions used for the model snapshot are the fractions of NO_x remaining multiplied by the emissions. The green column represents the emissions that are propagated in the regular model chemistry. **(b)** Simulated tropospheric NO_2 columns for a grid cell with ship emissions in the Bay of Biscay at 1 June 2005. The orange to red colours in the third bar represent the contribution to the column from emissions from the last 2.5 h, which are added to the background column to provide model output consistent with a satellite snapshot at 13:30 LT. As reference, the tropospheric NO_2 columns for this location without ship emissions (blue) and when using instant dilution (purple) are also given.

contributions from emissions that occurred during the past 2.5 h, we need to take these into account as well. Therefore, we extended our plume-in-grid approach solely for the model output between 13:00 and 15:00 LT. The continuous plume between release and 2.5 h prior was discretized in three parts (emissions between release and 0.5 h, between 0.5 and 1.5 h, and between 1.5 and 2.5 h). We multiply the emissions in these periods by the fraction of NO_x remaining after 15 min, 1 h and 2 h of plume expansion, respectively (Fig. 1a). These emissions are added to the NO_x concentration in the grid cell (Fig. 1b) and the resulting tropospheric columns are stored in order to allow for a fair comparison between the satellite observations (sensitive to all recent emissions) and GEOS-Chem. Note that the ship emissions from the last 2.5 h are not propagated in the regular model chemistry, but are only accounted for to provide a model snapshot that is representative of what the satellite observes.

To evaluate tropospheric NO_2 simulated with this extended plume-in-grid method, we compared against the conventional approach of instantly diluting NO_x emissions over a grid cell. Our simulation with the plume-in-grid approach (and accounting for fresh emissions) leads to a higher column than instant dilution (Fig. 1b). This is because just after initial release in the plume, OH concentrations are much suppressed, resulting in a longer NO_2 lifetime (during the first part of expansion), and as a result a higher NO_2 column. However, this is not always the case. Depending on ambient conditions (e.g. background NO_x and O_3 concentrations), the fraction of NO_x remaining (and hence the NO_2 column) can be either higher (Fig. 2a) or lower (Fig. 2b) than predicted by instant dilution. For the first hours of expansion, OH is suppressed in the plume, and the fraction of NO_x remaining for the expanding plume (solid line) is higher compared to instant dilution of emissions (dashed line). If NO_x and O_3 concentrations are relatively high (0.6 and 60 ppbv, respectively; Fig. 2a), the expanding plume simulated by the PARANOX Gaussian plume model (Vinken et al., 2011) results in a higher fraction of NO_x remaining compared to instant dilution. For relatively clean ambient conditions – NO_x and O_3 concentrations of 0.15 and 39 ppbv, respectively (Fig. 2b) – the expanding plume simulation has a lower fraction of NO_x remaining compared to instant dilution, as in this case the higher NO_x concentrations in the plume lead to efficient OH formation and a shorter NO_x lifetime. Figure 2b is consistent with a recent study by Valin et al. (2011), who showed, using a 2-D plume model, NO_2 columns for a $2 \times 2\,km^2$ (i.e. "plume" size) simulation could be higher (by up to 35 %) compared to $48 \times 48\,km^2$ (instant dilution scale) resolution simulations for a moderate emission strength. Furthermore, we note that horizontal transport of emissions in the 2.5 h of expansion is not included in Fig. 1b, while for instant dilution there is transport out of the grid cell in this time, resulting in a lower column. The effect of this transport on our final constraints is minor, as we use long temporal

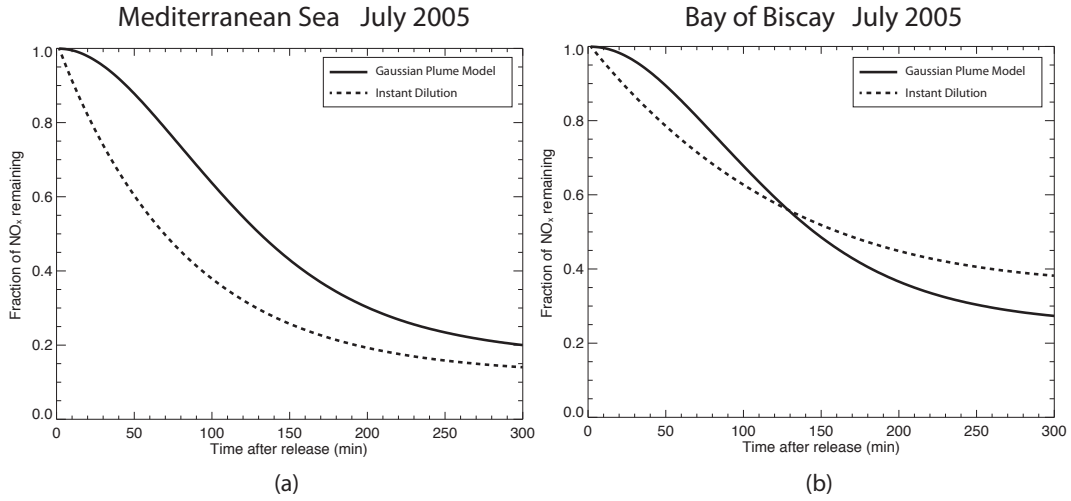

Fig. 2. Fraction of NO_x remaining as function of time calculated by the PARANOX Gaussian plume model (Vinken et al., 2011) for two representative cases in the Mediterranean Sea **(a)** and the Bay of Biscay **(b)** for July 2005. The solid line indicates the fraction of NO_x remaining in an expanding plume with initial size of $5 \times 5\,km^2$, and the dashed line represents an initial plume size of $50 \times 50\,km^2$ (approximating instant dilution).

averages and use enhanced NO_2 from ship emissions extended over multiple grid cells. Although the plume-in-grid approach presented in this work will probably introduce additional model errors, it takes into account non-linear chemistry in expanding ship emission plumes, allowing for an appropriate comparison of satellite observations and model simulations of aged pollution plumes.

2.2 Ozone Monitoring Instrument

The Dutch–Finish Ozone Monitoring Instrument (OMI) is a nadir-viewing solar backscatter imaging spectrograph aboard the Aura satellite, measuring in the range 264 to 504 nm (Levelt et al., 2006). Aura was launched in sun-synchronous polar orbit on 15 July 2004 with a local Equator-crossing time of 13:40 h. OMI measurements have a spatial resolution up to $13\,km \times 24\,km$ for nadir pixels and provide daily global coverage. We use the tropospheric NO_2 vertical column densities from Dutch OMI tropospheric NO_2 (DOMINO) v2.0 product (available from the Tropospheric Emissions Monitoring Internet Service (TEMIS); http://www.temis.nl). The DOMINO v2.0 product includes improvements in the radiative transfer modelling, high-resolution surface albedo climatology, better a priori TM4 NO_2 vertical profiles and high-resolution terrain height (Hains et al., 2010; Boersma et al., 2011). The uncertainty in OMI-observed columns due to spectral fitting is $0.7 \times 10^{15}\,molecules\,cm^{-2}$ and dominates the overall retrieval error over remote, unpolluted areas (Boersma et al., 2007). Errors arising from incorrect assumptions on surface albedo, aerosols, clouds or the NO_2 vertical profile dominate the overall retrieval error over polluted regions (Boersma et al., 2004). The total error budget for DOMINO v2.0 is estimated to be $1.0 \times 10^{15}\,molecules\,cm^{-2} + 25\,\%$ (Boersma et al., 2011). Recently, Irie et al. (2012) showed that only a small bias ($-10 \pm 14\,\%$) exists between DOMINO v2.0 retrievals and in situ multi-axis differential optical absorption spectroscopy (MAX-DOAS) observations at several sites in Japan and China.

The first step of retrievals on OMI data yields slant columns: the integrated abundance of NO_2 along the average photon path through the atmosphere to the instrument. These slant columns are converted to (tropospheric) vertical column densities (VCDs) using a (tropospheric) air mass factor (AMF). This AMF, and hence the retrieved tropospheric NO_2 VCD, is sensitive to the a priori vertical NO_2 profile. In the DOMINO v2.0 retrieval (from now on called DOMINO2), NO_2 vertical profiles simulated by TM4 (Dentener et al., 2003) are used. These vertical profiles have a native spatial resolution of $2° \times 3°$, which is improved upon by spatial interpolation to the OMI pixel centre. Here we replace these a priori vertical NO_2 profiles with profiles from GEOS-Chem nested-grid simulations ($1/2° \times 2/3°$ horizontal resolution) for the same day and (overpass) time of the OMI measurement, and calculate new tropospheric AMFs. Application of these new tropospheric AMFs results in a new data set of tropospheric VCDs (from now on called DOMINO2_GC), allowing a consistent comparison of the OMI-observed columns with GEOS-Chem-simulated columns, because the vertical distribution assumed in the retrieval is now the same as predicted by the model. The effect of these high-resolution GEOS-Chem profiles will be discussed in the next section.

We exclude clouded situations and snow- or ice-covered pixels to limit retrieval errors by filtering pixels with cloud radiance fraction above 0.5 and surface albedo above 0.2.

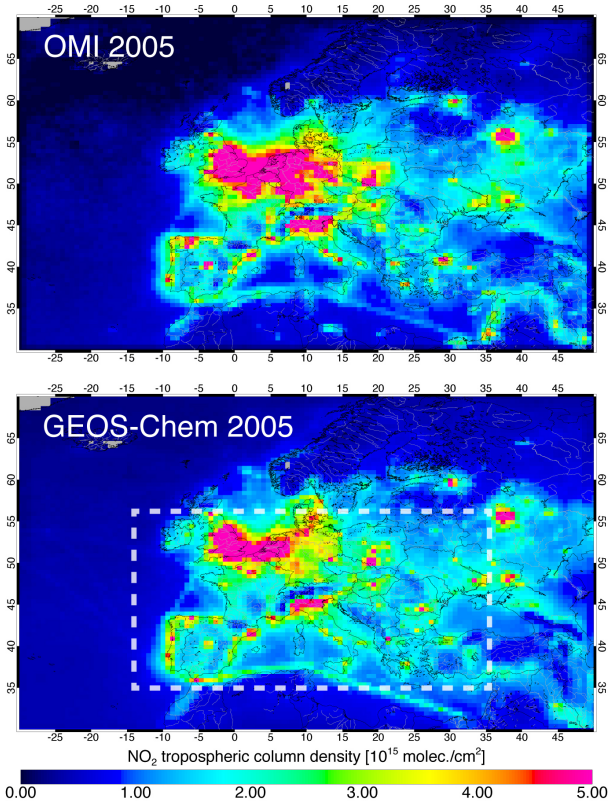

Fig. 3. Annually averaged tropospheric NO_2 columns on a $1/2^\circ \times 2/3^\circ$ resolution for OMI (DOMINO2_GC, top) and GEOS-Chem (bottom). Pixels with cloud radiance fraction above 0.5 and surface albedo above 0.2 are excluded to reduce retrieval errors. Furthermore the outer two pixels on each side of the swath are excluded. OMI pixels are regridded to the GEOS-Chem nested horizontal grid ($1/2^\circ \times 2/3^\circ$), requiring a grid cell coverage of over 75 % and more than three observations per grid cell. The dashed rectangle indicates the area over which spatial averages of OMI and GEOS-Chem are compared in Sect. 2.3.

The effective cloud fraction is obtained from the OMI O_2-O_2 retrieval (OMCLDO2) (Acarreta et al., 2004; Sneep et al., 2008), and OMI surface albedos are taken from Kleipool et al. (2008). We removed the outer two (large) pixels on each side of the swath to reduce spatial smearing due to viewing geometry. OMI pixels are regridded to the GEOS-Chem nested horizontal grid ($1/2^\circ \times 2/3^\circ$), requiring a grid cell coverage of over 75 % and that there are more than three observations per monthly/seasonal average. A 1 yr averaged map of OMI tropospheric NO_2 columns is shown in Fig. 3 for 2005.

2.3 Evaluation of GEOS-Chem and OMI tropospheric NO_2 columns

We compare GEOS-Chem simulations of tropospheric NO_2 columns with OMI-observed columns (both DOMINO2 and DOMINO2_GC) for 2005 (Figs. 3 and 4). Spatial patterns between DOMINO2_GC and GEOS-Chem for these annual averages over the entire domain are highly consistent ($R^2 = 0.90$, $n = 9270$), but the simulated columns are lower than DOMINO2_GC over urban and industrial areas. Although the observations show stronger seasonal variation for 2005–2006 (Fig. 4), the temporal correlation between GEOS-Chem and DOMINO2_GC monthly means ($R^2 = 0.95$) is remarkably strong, with a root-mean-square error (RMSE) of 0.24×10^{15} molec cm^{-2}. For GEOS-Chem and DOMINO2 the temporal correlation is $R^2 = 0.89$, with an RMSE of 0.45×10^{15} molecules cm^{-2}. Huijnen et al. (2010) found a spatial correlation of $R = 0.8$ ($n = 6000$) between an ensemble median of regional air quality models and OMI NO_2 observations (DOMINO v1.0.2) over the same domain as in this study for 2008–2009. Furthermore, Huijnen et al. (2010) found that the ensemble median underestimates NO_2 columns by up to 50 % in summer, with only a small bias in winter. The GEOS-Chem model agrees better to OMI observations, reflecting the improved (lower) uptake coefficient for N_2O_5 on aerosols (Sect. 2.1) and DOMINO NO_2 retrievals (v2.0).

Differences between DOMINO2_GC and DOMINO2 (Fig. 5) arise from the different a priori NO_2 profiles used in the air mass factor (AMF) calculation. GEOS-Chem NO_2 profiles differ in three ways from the original TM4 profiles: (1) different emissions over the domain, (2) higher spatial resolution and (3) a different CTM (e.g. different vertical mixing and chemical lifetime). Different emissions most likely dominate the changes in AMFs. TM4 used emissions from the POET project (Precursors of Ozone and their Effects on the Troposphere) for the year 1997 (Olivier et al., 2003), which amount to 8.2 Tg N yr^{-1} for Europe. In GEOS-Chem we use EMEP (Vestreng et al., 2007) emissions, which amount to 6.3 Tg N yr^{-1} for 2005. Lower emissions lead to lower concentrations in the a priori profiles (Fig. S1), and hence higher AMFs (Fig. S2), resulting in lower tropospheric NO_2 columns (e.g. Martin et al., 2003; Boersma et al., 2004), as can be observed by the reduction in NO_2 columns over western Europe in Fig. 5. In contrast, increased emissions in eastern Europe lead to increased OMI NO_2 columns here. This dependence of AMFs on a priori emissions in the retrieval profiles was earlier found by Barkley et al. (2012) for HCHO vertical columns. The effect of the higher resolution of the GEOS-Chem profiles can be observed near large cities (e.g. Barcelona), where NO_2 columns increase due to better localized emissions in the NO_2 profiles.

OMI NO_2 retrievals using GEOS-Chem NO_2 profiles in the AMF calculation are on average 10 % lower than the original DOMINO2 retrievals using TM4 a priori NO_2 profiles. The new DOMINO2_GC retrievals and GEOS-Chem now agree to within 7 %, with largest differences in winter months. The wintertime underestimation of GEOS-Chem shown in Fig. 4 possibly reflects a too short NO_2 chemical lifetime in GEOS-Chem, as suggested by a number of recent studies on reaction rate updates (e.g. Stavrakou et al.,

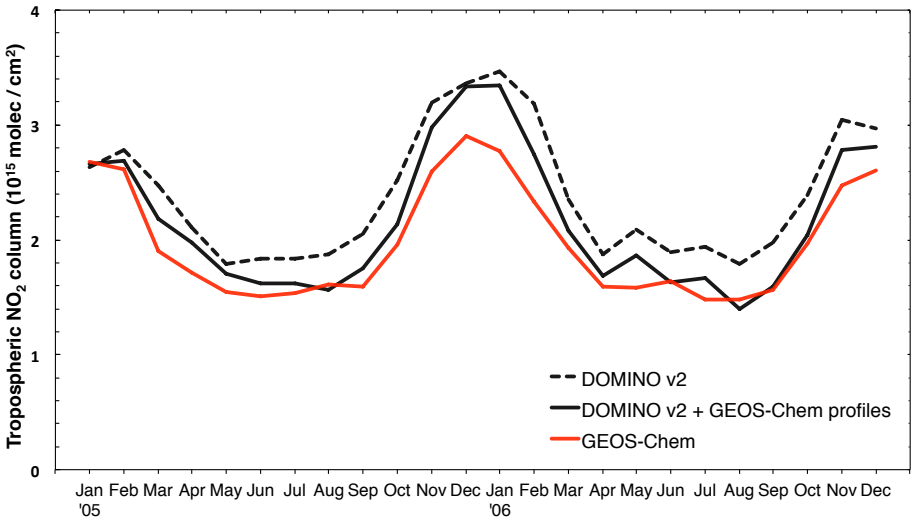

Fig. 4. Comparison of monthly averaged OMI and GEOS-Chem tropospheric NO_2 columns for 2005–2006 averaged over (central) Europe defined in Fig. 3. Selection of OMI observations follows the same criteria as Fig. 3.

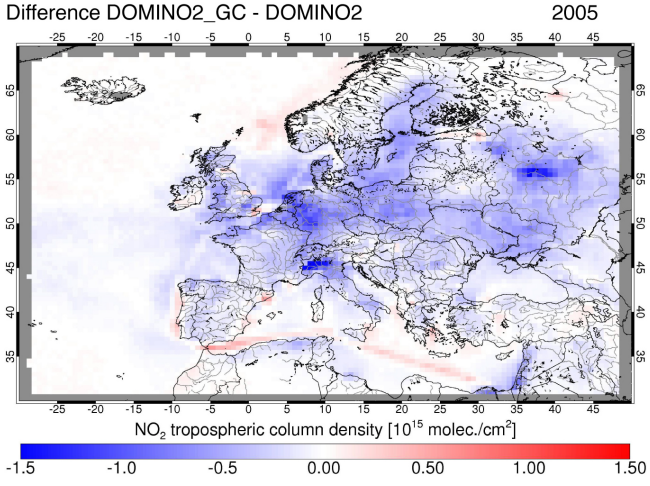

Fig. 5. Differences between annually averaged OMI NO_2 columns for 2005 on a $1/2° \times 2/3°$ resolution using the DOMINO2_GC retrieval (with a priori NO_2 profiles based on GEOS-Chem $1/2° \times 2/3°$ simulations) and DOMINO2 retrieval (with a priori profiles based on TM4 $2° \times 3°$ simulations). Selection of OMI observations follows the same criteria as Fig. 3. Differences between these two retrievals arise from different a priori NO_2 profiles, as discussed in Sect. 2.3. The AMFs for these retrievals are shown in Fig. S2.

2013; Zhang et al., 2012). In particular, the value for the uptake coefficient $\gamma_{N_2O_5}$ in GEOS-Chem is high compared to recent laboratory and field estimates of this value (e.g. Brown et al., 2009; Mollner et al., 2010; Henderson et al., 2012; Butkovskaya et al., 2007, 2009). We conclude that the nested GEOS-Chem CTM is in close agreement with OMI-observed NO_2 columns over Europe. Differences in wintertime between OMI and GEOS-Chem are unlikely to influence our results because of our filter criteria (discussed in the next section).

2.4 Selection of OMI NO_2 observations

Figure 3 (top) shows two ship tracks in the annually averaged OMI NO_2 observations: one in the Bay of Biscay and one in the Mediterranean Sea. Emission inventories (see next section) suggest that there are also busy ship routes in the North Sea. However, detection of ship tracks in this sea presents significant challenges, since influence from outflow of pollution from land often prohibits a clear view of the pollution from ships. To be able to detect ship emissions in this sea, we inspect daily OMI observations and screen out all days with measurements that are significantly affected by continental outflow (e.g. Fig. 6a). Furthermore, we filter for days that have cloud-free observations (cloud radiance fraction < 0.5) over at least 90% of the ship track area (Fig. 6b), as scattered clouds prevent the unambiguous detection of pollution from ships. In addition to this cloud filter, we also exclude strong negative NO_2 columns ($< -0.5 \times 10^{15}$ molecules cm^{-2}). Using these two criteria we can now identify two additional ship tracks in European seas (the Baltic Sea and the North Sea) (Fig. 6c).

3 Top-down ship emission estimates

3.1 Ship emission inventories

In the GEOS-Chem CTM two (recent) ship emission inventories can be used for Europe: the European regional EMEP inventory (Vestreng et al., 2007) and the global AMVER-ICOADS inventory (Wang et al., 2008). The left panels of Fig. 7 show the spatial distribution of European ship NO_x

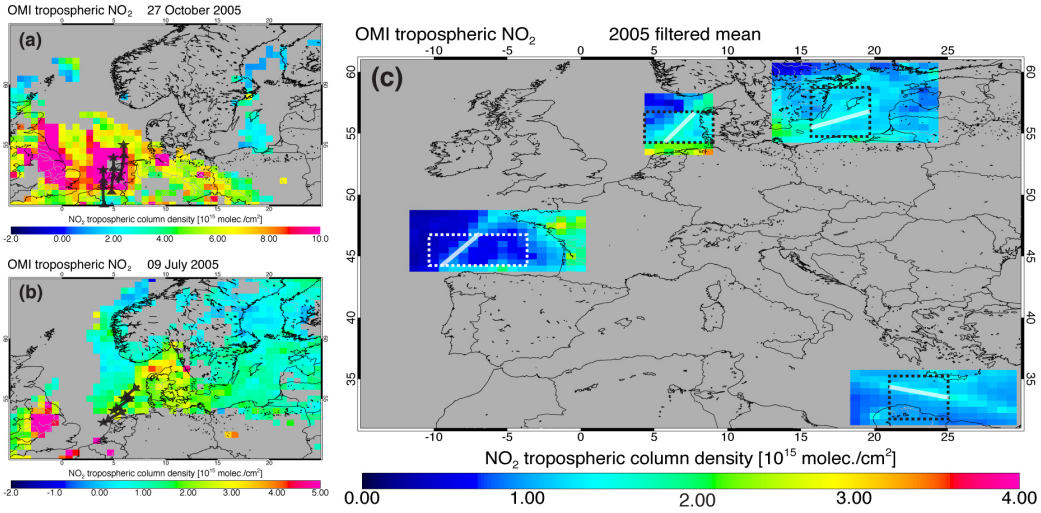

Fig. 6. (a) OMI NO_2 observation over the North Sea influenced by outflow from land (note different scale). Back trajectories with the NOAA-HYSPLIT model show that the North Sea air originated from the Netherlands (black arrows and stars). **(b)** OMI NO_2 observation with cloud-free observations over the entire North Sea (and Baltic Sea). North Sea air originated from the clean sea for this day (back trajectories in black arrows and stars). **(c)** Four ship tracks are visible in the resulting annual average for 2005, after screening out days with partial coverage of the area and strong outflow (background NO_2 columns adjacent to the ship tracks larger than 2×10^{15} molecules cm^{-2} for the North Sea, the Baltic Sea and the Mediterranean Sea, and larger than 1.5×10^{15} molecules cm^{-2} for the Bay of Biscay). The number of days included in this filtered mean is largest for the Mediterranean Sea (about 100), and lower for other seas (the North Sea: 20; the Baltic Sea: 45; the Bay of Biscay: 35). Dashed boxes indicate the ship track areas that were used to calculate constraints in this study, and ship tracks were averaged along the white lines in these boxes.

emissions, with totals for the EMEP and AMVER-ICOADS inventory for 2005 of 1.1 and 0.8 Tg N, respectively. Differences between these inventories arise from the use of different methodologies (e.g. using fuel consumption versus shipping activity) and spatial allocation. The AMVER-ICOADS inventory is based on international fuel statistics, which do not include fuel consumed for domestic traffic, whereas EMEP does include these domestic emissions. Therefore AMVER-ICOADS underestimates ship emissions over inland seas and coastal zones with significant domestic ship traffic, like the (eastern part of the) Mediterranean Sea (Marmer et al., 2009). The spatial allocation in EMEP is based on the distance each ship covers between ports, information provided by the Lloyd's Register of Shipping (Vestreng, 2003). In the AMVER-ICOADS inventory the spatial allocation is taken from actual ship locations reported to the Automated Mutual-Assistance Vessel Rescue System (AMVER) and International Comprehensive Ocean-Atmosphere Data Set (ICOADS). Comparison with annual OMI NO_2 observations (Fig. 7b) for the eastern part of the Mediterranean Sea shows that the AMVER-ICOADS inventory (Fig. 7c) simulates the ship track closer to the observed tracks. The location of the EMEP emissions is misplaced by up to 150 km (too close to Crete, Fig. 7a). However, as the EMEP inventory does include domestic ship traffic, we combine both inventories and generate a new ship emission inventory (Fig. 7d). This inventory is based on EMEP emission totals, and AMVER-ICOADS emission locations for the eastern part of the Mediterranean Sea. In the following, we will use the combined EMEP & AMVER-ICOADS database as the a-priori emission inventory in our simulations.

3.2 Sensitivity of GEOS-Chem NO_2 columns to NO_x emissions

Within pollution plumes, the NO_x lifetime is influenced by the local NO_x concentration. This is because oxidation losses depend on in-plume OH availability, which is determined by the local concentration of pollution, e.g. the NO_x concentration itself. We need to account for this non-linear feedback when changing NO_x emissions based on observed (changes in) NO_2 columns. Lamsal et al. (2011) introduced a dimensionless factor β, which represents the (modelled) local sensitivity of NO_2 column changes to NO_x emissions changes. β is computed by changing NO_x emissions by a fixed prescribed percentage and evaluating the local (relative) change in NO_2 column:

$$\beta = \frac{\Delta E / E}{\Delta N_{GC} / N_{GC}}, \quad (1)$$

where E represents the NO_x emissions, N_{GC} the simulated tropospheric NO_2 column, ΔE the change in NO_x emissions and ΔN_{GC} the subsequent change in simulated tropospheric NO_2 column. Lamsal et al. (2011) found a global mean β value of 1.16 when perturbing emissions by 15 %. β tends to be greater than 1 in remote areas with relatively

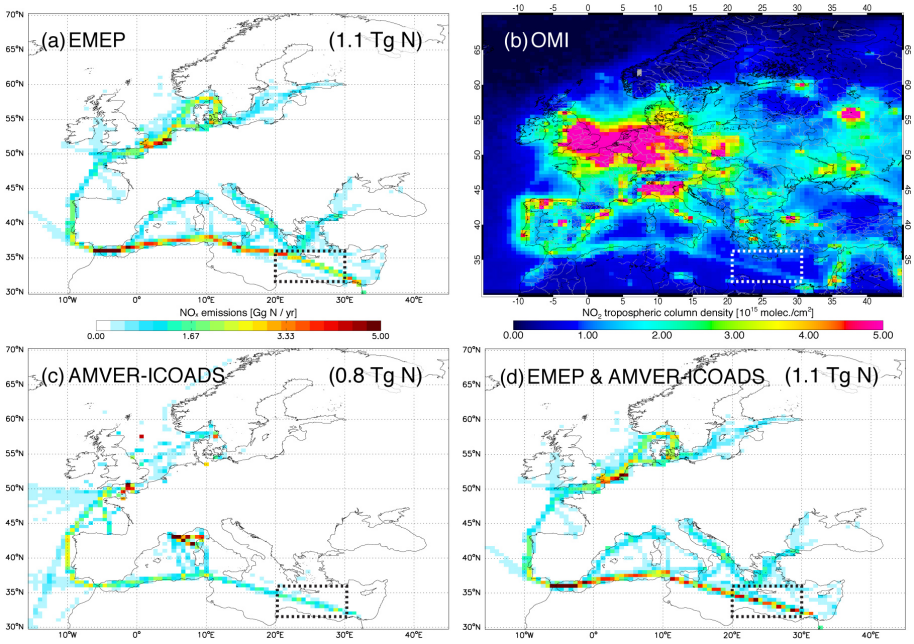

Fig. 7. EMEP (Monitoring and Evaluation of the Long-range Transmission of Air Pollutants in Europe) NO_x ship emission inventory (Vestreng et al., 2007) for 2005, showing emissions in the Mediterranean Sea close to Crete (**a**, black rectangle). In the AMVER-ICOADS inventory (Wang et al., 2008) for 2001 **(c)**, the location of emissions in the Mediterranean Sea is closer to the ship track location visible in an annual average of OMI tropospheric NO_2 columns for 2005 **(b)**. For this study we created a combination of the EMEP and AMVER-ICOADS inventory, replacing EMEP emissions in the Mediterranean Sea by AMVER-ICOADS emissions, scaled to the EMEP total over this area **(d)**.

low NO_2 concentrations, reflecting efficient OH production and a lower NO_x lifetime following an increase in emissions. In polluted areas, β tends to be less than 1 as an increase in NO_x will consume OH and increase the NO_x lifetime. Recently, Lu and Streets (2012) showed a decrease of β values from about 2 to 0.7 over Indian power plants during the period 1996–2010, following a dramatic increase in NO_x emissions. Their study illustrates the strong variability of β, and the need to determine β for a realistic emission strength. We calculate β from seasonal mean NO_2 columns (over the entire ship track as defined in Fig. 6) for the Mediterranean Sea, and from annual mean columns for the Bay of Biscay, the North Sea and the Baltic Sea (filtered by the criteria of Sect. 2.4). As we expect our ship emissions to change by more than 15 % we follow a two-step approach to calculate β values, different from Lamsal et al. (2011). First we run our model with emissions perturbed by the relative difference of observed and simulated NO_2 columns (ignoring the non-linear feedback of emission on simulated columns). From the results of these simulations we calculate β values for our ship tracks and apply these to derive new top-down emissions. We find β values of 0.3–0.9 (Table 2), indicating that emission changes lead to substantial changes in NO_2 columns over the ship lanes. This is expected, as ship emissions are released following our plume-in-grid approach, and NO_x concentrations will be relatively high in the expanding plume, a situation comparable to release of NO_x in a polluted area. Differences in β are driven by the magnitude of emissions changes and local chemical regime. For example, in the Baltic Sea we impose strong emissions perturbations, and the resulting β values are small (comparable to a decreasing β from $\sim$2 to $\sim$0.7 found in Lu and Streets (2012) for increasing emissions of power plants). Emissions changes for the North Sea and the Mediterranean Sea are similar; however the calculated β values ($\sim$0.6 for the North Sea, $\sim$0.8–0.9 for the Mediterranean Sea) indicate different chemical regimes. This is consistent with Fig. S1 in Lamsal et al. (2011), which indicates that β values are lower for wintertime and polluted areas, and higher β values correspond with summer and less polluted areas.

3.3 Sensitivity of OMI NO_2 columns to a priori (GEOS-Chem) NO_2 columns

OMI tropospheric NO_2 columns depend on the a priori vertical NO_2 profile. In this study we replaced the TM4 profiles used in the DOMINO v2.0 retrieval with high-resolution GEOS-Chem-simulated NO_2 profiles (Sect. 2.2, leading to OMI NO_2 retrievals 10 % lower than original DOMINO2). As a result of constraining ship emissions in GEOS-Chem, the retrieved OMI NO_2 columns will also change in response to updated a priori NO_2 profiles over the shipping lanes. We quantify the effect of changing GEOS-Chem NO_2 columns

Table 2. Overview of total ship NO_x emissions for different ship tracks (as defined in Fig. 9b): in the EMEP and AMVER-ICOADS emission inventories, and our OMI top-down inventory for 2005–2006. For the North Sea, the Baltic Sea and the Bay of Biscay, annual constraints are given. More cloud-free observations are available for the Mediterranean Sea and we provide seasonal constraints for this ship track, although winter constraints could not be determined. Beta and gamma values are calculated as indicated in Sects. 3.2. and 3.3. Note that the combined EMEP-AMVER-ICOADS inventory (Fig. 7d) used in this study has the same emission totals as the EMEP inventory.

Ship track*	Season/ Year	Initial relative difference $\frac{N_{OMI,1}-N_{GC,1}}{N_{GC,1}}$	β_1 value	γ_1 value	EMEP (Tg N)	OMI top-down (Tg N)	AMVER-ICOADS (Tg N)
North Sea (4.7° E, 54.5° N) – (11.3° E, 54.5° N)	2005	−0.39	0.58	0.59	0.08	0.05	0.02
	2006	−0.32	0.55	0.57	0.08	0.06	0.02
Baltic Sea (14.7° E, 54.5° N) – (25.3° E, 60° N)	2005	1.91	0.25	0.16	0.02	0.05	0.003
	2006	1.99	0.27	0.18	0.02	0.06	0.003
Bay of Biscay (10° W, 43.5° N) – (3.3° W, 50° N)	2005	1.01	0.74	0.29	0.04	0.08	0.05
	2006	1.30	0.64	0.26	0.04	0.09	0.05
Mediterranean Sea (6° W; 36° N) – (31.7° E; 31.5° N)	Spring 2005	−0.46	0.88	0.64	0.08	0.02	0.03
	Summer 2005	−0.45	0.95	0.84	0.08	0.02	0.03
	Autumn 2005	−0.47	0.81	0.43	0.08	0.03	0.03
	Annual 2005	−0.46	0.88	0.64	0.32	0.10	0.13
	Spring 2006	−0.37	0.85	0.57	0.08	0.03	0.03
	Summer 2006	−0.47	0.8	0.87	0.08	0.02	0.03
	Autumn 2006	−0.38	0.79	0.45	0.08	0.04	0.03
	Annual 2006	−0.41	0.81	0.63	0.30	0.13	0.13

* Relative difference, β and γ are calculated over the areas defined in Fig. 6c. Emission strengths are summed over the constrained ship tracks as indicated in Fig. 9d.

(NO_x emissions) on OMI NO_2 columns by introducing a dimensionless factor γ:

$$\gamma = \frac{\Delta N_{OMI}/N_{OMI}}{\Delta N_{GC}/N_{GC}}, \quad (2)$$

where N_{GC} represents the simulated tropospheric NO_2 column corresponding to the a priori profile shape used in the retrieval, N_{OMI} the retrieved OMI tropospheric NO_2 column, ΔN_{GC} the change in simulated NO_2 column as a result of changing emissions, and ΔN_{OMI} the change in retrieved NO_2 column because of the changed a priori NO_2 profile. A γ value of zero would indicate no sensitivity of OMI NO_2 columns to changing GEOS-Chem columns. We calculate γ values in the same way as β values using results of a model run with perturbed emissions. γ is found to be always smaller than 1 (Table 2), indicating that the relative change in OMI NO_2 column from a priori is always smaller than the relative change in a priori GEOS-Chem columns. The γ factor not equal to zero illustrates that OMI retrievals are never completely independent of a priori assumptions, and this factor takes into account how the changing profile shape influences our retrieval.

3.4 Space-based constraints on ship emissions

Figure 6c shows a map of OMI tropospheric NO_2 columns for 2005, gridded on the GEOS-Chem horizontal resolution ($1/2° \times 2/3°$). The conventional approach (Martin et al., 2003; Lamsal et al., 2011) to estimate top-down NO_x emissions ($E_{top\,down}$) for the four major ship routes that are visible in the Baltic Sea, the North Sea, the Bay of Biscay and the Mediterranean Sea would be to use the relative difference of observed and simulated columns (using the a priori emissions, indicated by the subscript 1) over these ship routes in combination with the modelled sensitivity β_1 to scale the a priori emissions:

$$E_{top\,down} = E_{a\,priori} + \left(\frac{N_{OMI,1} - N_{GC,1}}{N_{GC,1}}\right) \cdot \beta_1 \cdot E_{a\,priori}. \quad (3)$$

In this study, we determine β_1 by perturbing the a priori ship emissions by the relative difference of observed and simulated columns:

$$\beta_1 = \frac{\Delta E/E}{\Delta N_{GC}/N_{GC,1}} = \frac{(N_{OMI,1} - N_{GC,1})/N_{GC,1}}{(N_{GC,2} - N_{GC,1})/N_{GC,1}},$$

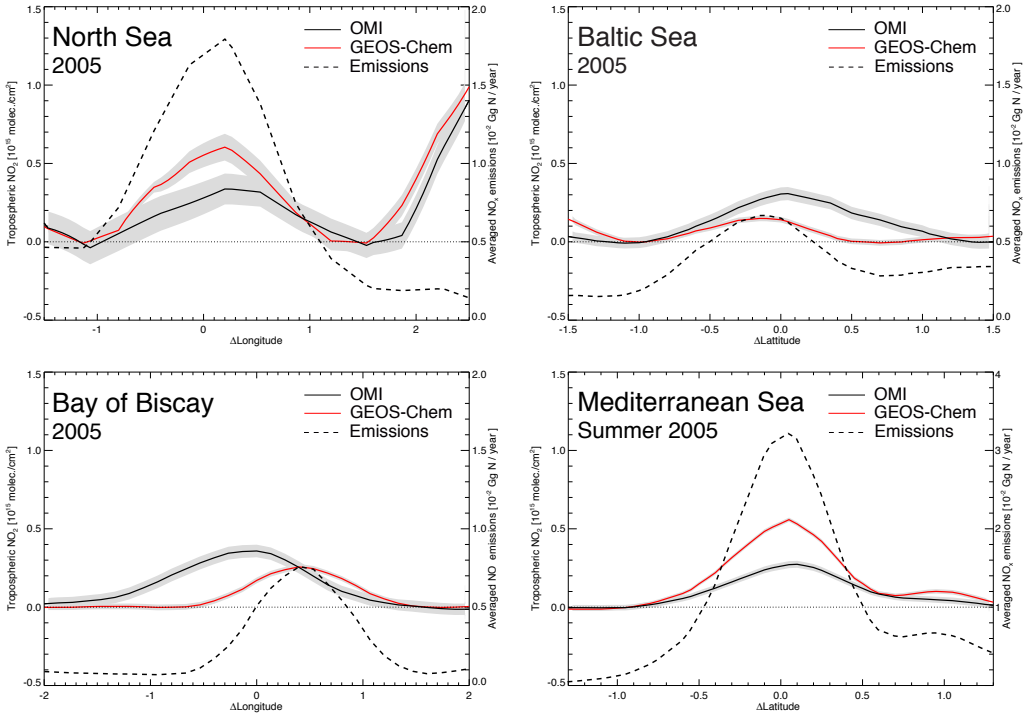

Fig. 8. Along-ship-track averages of tropospheric NO_2 columns over the areas in Fig. 6c for observed columns by OMI (black line), and simulated columns by GEOS-Chem (red line). The area was averaged over longitude for the Baltic Sea (between 16 and 19.33° E, upper right) and the Mediterranean Sea (21.33 to 24.67° E, bottom right), and over latitude for the North Sea (54.5 to 56.5° N, upper left) and the Bay of Biscay (44.5 to 46.5° N, lower left). Emissions averaged along the ship track are represented by the dashed line. A linear background fit was subtracted from the averages, and grey shading represents the sample standard error.

where $N_{GC,2}$ represents the GEOS-Chem-simulated column after perturbing the a priori ship emissions by the factor $((N_{OMI,1} - N_{GC,1})/N_{GC,1})$.

γ_1 was determined following Eq. 2 by means of

$$\gamma_1 = \frac{(N_{OMI,2} - N_{OMI,1})/N_{OMI,1}}{(N_{GC,2} - N_{GC,1})/N_{GC,1}},$$

where $N_{OMI,2}$ represents the OMI tropospheric NO_2 column retrieved with the NO_2 profile of the perturbed GEOS-Chem simulation (simulation 2). Replacing the NO_2 profile in the OMI NO_2 retrieval is comparable to replacing the TM4 a priori profiles by GEOS-Chem profiles in the DOMINO2_GC retrieval (see Sect. 2.3 and the Supplement for a discussion of the effect).

We now extend the approach by Lamsal et al. (2011) (Eq. 3) by also taking into account the sensitivity of the OMI retrievals to changes in a priori NO_2 profiles. We do so by adding a term to Eq. 3 that accounts for the response of the retrieval to the changed emissions and modifies the overall scaling of the a priori inventory by $((N_{OMI,1} - N_{GC,1})/N_{GC,1}) \cdot \gamma_1 \cdot \beta_1$.

The new top-down NO_x emissions inventory we then obtain via

$$E_{\text{top down}} = E_{\text{a priori}} + \left(\frac{N_{OMI,1} - N_{GC,1}}{N_{GC,1}}\right) \cdot \beta_1 \cdot E_{\text{a priori}} \quad (4)$$
$$+ \left(\frac{N_{OMI,1} - N_{GC,1}}{N_{GC,1}}\right) \cdot \gamma_1 \cdot \beta_1 \cdot E_{\text{a priori}}.$$

The second term on the right-hand side of Eq. (4) describes the scaling of the a priori emissions required to match the original observed ($N_{OMI,1}$) and simulated ($N_{GC,1}$) NO_2 columns. The third term on the right-hand side may be interpreted as a necessary enhancement of the second term: an increase in a priori emissions by the factor $((N_{OMI,1} - N_{GC,1})/N_{GC,1}) \cdot \beta_1$ would lead to more pronounced a priori NO_2 profiles that in turn lead to lower AMFs and higher OMI-retrieved NO_2 columns by a factor $((N_{OMI,1} - N_{GC,1})/N_{GC,1}) \cdot \gamma_1$. In practice, the third term is always smaller than the second term, but still leads to substantial emissions enhancements of up to 35 % on top of the second term (i.e. the approach of (Lamsal et al., 2011)).

We found that for the Baltic Sea, and in some seasons for the Mediterranean Sea, emission changes were large and an additional iteration was needed. For this additional iteration we applied Eq. (4) again, but now using the top-down emissions (calculated using Eq. 4) as a priori emissions and

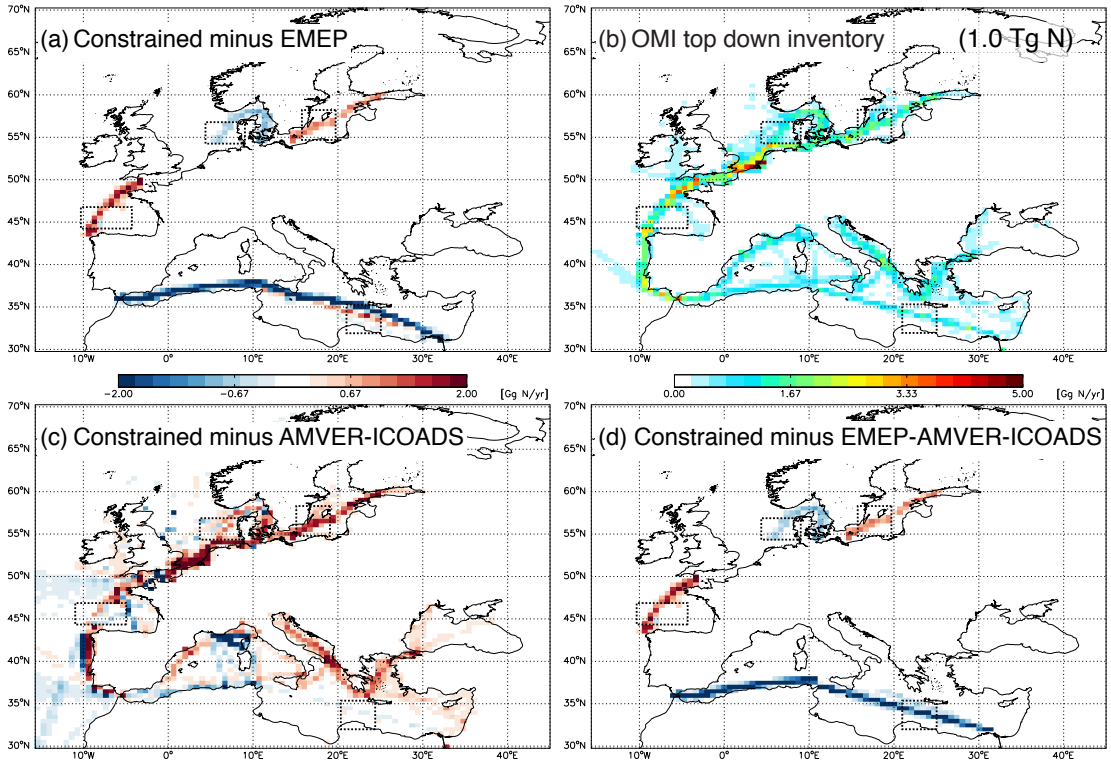

Fig. 9. Absolute difference in $Gg\,N\,yr^{-1}$ between the OMI top-down ship NO_x inventory for 2005 **(b)** and the EMEP-AMVER-ICOADS inventory **(d)**, indicating the ship tracks that were constrained in this study. Differences between the new top-down inventory and the (global) AMVER-ICOADS inventory **(c)** show good agreement in the Mediterranean Sea, but also show the lack of domestic ship traffic emissions in coastal waters. Comparison with the original EMEP inventory **(a)** shows the mislocated ship emissions in the Mediterranean Sea, as was discussed in Sect. 3.1. Dashed boxes indicate the ship track areas that were used to calculate constraints in this study.

also basing the OMI and GEOS-Chem columns on these top-down emissions (this additional iteration is described in the Supplement).

For the Baltic Sea, the North Sea and the Bay of Biscay we provide annual constraints based on annual averages of filtered days in 2005 and 2006 (see Sect. 2.4 for selection criteria). For the Mediterranean Sea, more days satisfying our criteria are available, allowing us to provide seasonal constraints for 2005 and 2006.

Using the seasonally and annually averaged tropospheric NO_2 columns, four along-ship-track averages were created by averaging the areas in Fig. 6c over the longitude for the Mediterranean Sea and the Baltic Sea, and over the latitude for the North Sea and the Bay of Biscay (Fig. 8). For these averages, these grid cells were rotated and interpolated along the ship track location. A linear background was fitted to these averages as indicated in Fig. S3 and subtracted from the cross sections. We use this background correction for both OMI and GEOS-Chem, ensuring consistency in the comparison. Using a simulation without ship emissions to determine the contribution of ships could lead to interpretation errors due to non-linearities in the NO_x chemistry. The averages clearly show enhanced columns relative to the background (of up to 0.6×10^{15} molecules cm^{-2}) over the ship routes. OMI observations indicate that NO_x emissions in GEOS-Chem are too low over the Baltic Sea and the Bay of Biscay, while emissions are too high over the North Sea and the Mediterranean Sea. Furthermore, the cross section for the Bay of Biscay (Fig. 8, left bottom) shows that emissions in GEOS-Chem are located too far to the east by 0.5° (or ~ 50 km), compared to the OMI observations. As our inversion does not correct the location of the emissions, we shifted the emissions prior to the inversion in the (combined) inventory to match the OMI location (see next section).

3.5 Top-down NO_x ship emissions

We proceed and determine the relative difference of the area under the OMI-observed and GEOS-Chem-modelled tropospheric NO_2 cross sections in Fig. 8. We use this relative difference $((N_{OMI,1} - N_{GC,1})/N_{GC,1})$ to provide constraints following Eq. (4) for sections of the four ship tracks indicated in Fig. 9. We apply these constraints to the much longer tracks shown in Fig. 9d assuming that the constraints for the sections are representative of the full shipping lane. These ship tracks amount to 39 % of all ship emissions in the EMEP ship emission inventory for Europe (by mass N). Due to the

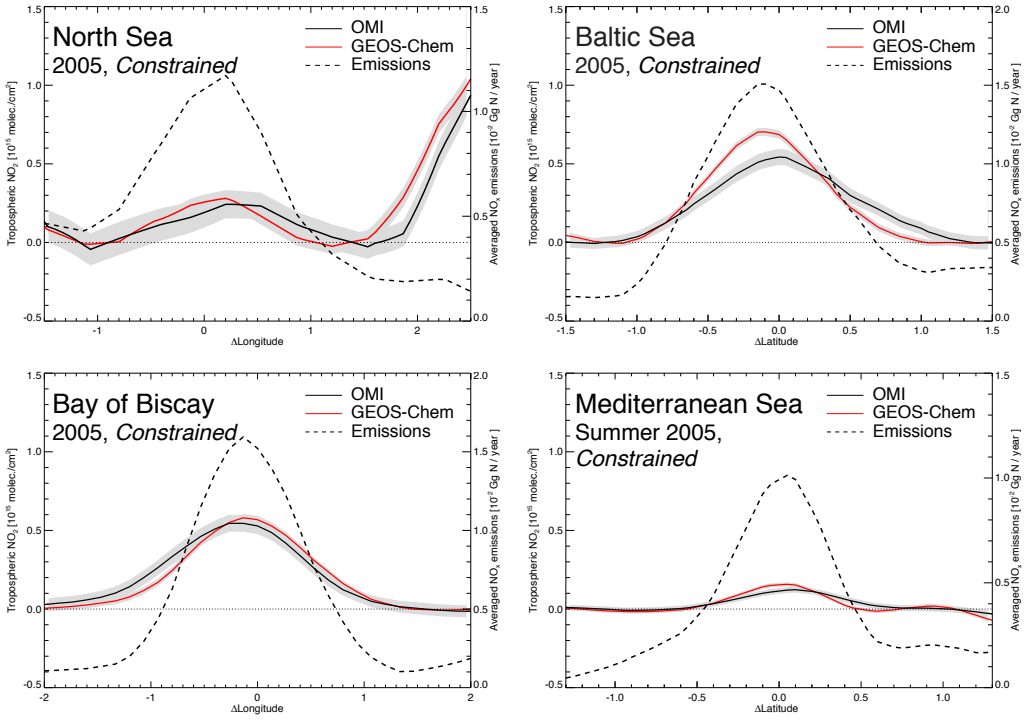

Fig. 10. Along-ship-track averages of the tropospheric NO_2 columns over the areas in Fig. 6c for observed columns by OMI (black line), and simulated columns by GEOS-Chem (red line) using constrained emissions of Fig. 9b. OMI tropospheric NO_2 columns were retrieved using a priori NO_2 profiles simulated with the new top-down emissions (see Fig. S1 and S2). Emissions averaged along the ship track are represented by the dashed line. The area was averaged over longitude for the Baltic Sea and the Mediterranean Sea (upper and bottom right) and over latitude for the North Sea and the Bay of Biscay (upper and lower left). A linear background fit was subtracted from the averages (see Fig. S3), and grey shading represents the sample standard error.

strong changes in emissions in some ship tracks and strong non-linearities in the NO_x chemistry, an additional iteration was needed to match the modelled columns to the simulated ones (see Table S1). This second iteration results in a close match (within 10 %) between observed and simulated column enhancements relative to background for all four ship tracks.

Figure 9 shows the results of our constraints on the ship NO_x emissions. The OMI top-down total ship NO_x emissions amount to 0.96 Tg N for 2005 (1.0 Tg N for 2006), a reduction of 15 % (11 %) compared to the EMEP inventory. The new inventory (Fig. 9b) is more coherent than the EMEP inventory (Fig. 7d), as sudden stepwise jumps in NO_x emissions, for instance from the Bay of Biscay to the ship lane west of Portugal, no longer appear. Emission totals for the four constrained European ship tracks are given in Table 2; these show that emissions in the Mediterranean Sea ship track are strongly reduced (to 0.13 Tg N) and closely match AMVER-ICOADS emissions (0.12 Tg N) for 2005 and 2006. Also the strong emissions in the North Sea track are reduced to 0.05 Tg N for 2005 (35 % lower than EMEP) and are more consistent with emission strengths in the Baltic Sea. Figure 9c shows that the AMVER-ICOADS inventory underestimates emissions in the North Sea and the Baltic Sea, and also illustrates that this inventory does not take into account domestic ship traffic in coastal zones. Our top-down emissions are still strong in the English Channel, but our satellite observations do not provide constraints for this area. We note that the TNO-MACC European emission inventory (Denier van der Gon et al., 2011) provides high-resolution ship emissions in the North Sea using ship location (automatic identification system) data (Jalkanen et al., 2009). OMI top-down emissions for the Baltic Sea and the Bay of Biscay ship tracks are 0.05 Tg N for 2005 (131 % higher than EMEP) and 0.08 Tg N for 2005 (128 % higher than EMEP), respectively. The constraints found in this study are also applied to the SO_x and CO emission inventories, assuming that the scaling in NO_x emissions is due to increased/decreased activity, and not due to changes in emissions factors.

Using simulations with our new top-down emission inventory, four along-ship-track averages of observed and simulated NO_2 columns were created (Fig. 10). Compared to Fig. 8, simulated columns now closely match (within 10 %) observed columns. Figure 10 also shows the emission strength averaged along the ship tracks. Emission strengths are similar in the Bay of Biscay and the Baltic Sea, but NO_2 column enhancements over ship lanes differ. NO_2 column enhancements are a factor of 3–4 lower over the

Mediterranean Sea compared to the Baltic Sea and the Bay of Biscay, while emissions are only 50 % lower, indicating different photo-chemical regimes (longer NO_2 lifetimes) in different seas in Europe.

3.6 Error of the top-down emission inventory

Our approach to derive new top-down ship NO_x emissions is sensitive to errors in both the satellite-observed and simulated NO_2 columns. Important systematic errors in the simulations have been addressed by taking into account the effects of non-linear chemistry in the expanding ship plume and by changing the location of emissions in the top-down inventory for the Mediterranean Sea and the Bay of Biscay. However, other systematic model errors may still persist, related to errors in the NO_2 chemistry (and hence lifetime), and (vertical) transport (e.g. Lin et al., 2012; Stavrakou et al., 2013). Our plume-in-grid method may also introduce errors in our approach, and we cautiously estimate these to be of the order of 15 %. OMI NO_2 observations also have systematic errors, due to errors in the AMFs or stratospheric correction. The error in an OMI-observed NO_2 column is estimated to be 1×10^{15} molecules cm^{-2} +25 %, and consists of a systematic and a random part (Boersma et al., 2011; Irie et al., 2012). We reduce random errors in OMI observations by averaging, but might also introduce an additional error in the background correction of our along-ship-track averages (Figs. 8 and 10), resulting in an estimate of OMI-related errors of 20 %. Effects of tighter cloud filtering (cloud radiance fraction < 0.25) are found to result in changes smaller than 10% for the Baltic Sea, and negligible differences for the Mediterranean Sea, the Bay of Biscay and the North Sea . This cloud-related uncertainty is included in the OMI-related error and estimated to be less than 10 %, in agreement with earlier results found for shipping NO_2 columns by Franke et al. (2009). Assuming the errors in OMI, GEOS-Chem and PARANOX to be largely uncorrelated, and using simple error propagation, we estimate the total systematic component of the errors in our approach to be 29 %. Apart from systematic errors in our model or observations, there are also random errors resulting from our approach. These errors arise from statistical errors in the averaging of the columns and determination of the relative difference between (background-corrected) observed and simulated columns. We used the sample standard error to calculate the statistical error in our averages. This error is lowest (30 %) in summer months for the Mediterranean Sea, when a large number of observations are available. The statistical error for the North Sea track is largest (70 %), as NO_2 columns will show more variation due to close proximity to polluted areas. Overall we estimate an error of 40–60 % on our OMI top-down ship NO_x emissions inventory.

4 Conclusions

We developed a method to constrain a large fraction (39 %) of European ship NO_x emissions using OMI tropospheric NO_2 columns and the nested-grid GEOS-Chem CTM in the Baltic Sea, the North Sea, the Bay of Biscay and the Mediterranean Sea. Our method allows for a direct comparison between satellite-observed and simulated NO_2 columns (using a model snapshot). First, we updated our previously developed plume-in-grid approach, which accounts for non-linear chemistry in expanding ship plumes for GEOS-Chem ($1/2^\circ \times 2/3^\circ$ resolution). OMI showed that ship emissions were misplaced in the Mediterranean Sea and the Bay of Biscay, and we made sure ship emissions were released at the correct location in the CTM. These updates reduce systematic errors in our simulations. Second, we ensured consistency between retrieval and modelling by replacing TM4 a priori NO_2 profiles by high-resolution GEOS-Chem profiles. To reduce influence of continental pollution, and improve detection of ship tracks, we screened out observations that were affected by outflow. Furthermore we only included days that have cloud-free observations over the entire ship track. As a result, we are able to identify ship tracks in four European seas (the Baltic Sea, the North Sea, the Bay of Biscay and the Mediterranean Sea). This is the first time that ship tracks in the Baltic Sea, the North Sea and the Bay of Biscay have been observed in OMI tropospheric NO_2 columns and used to constrain ship NO_x emissions.

We use the relative difference between observed and simulated NO_2 columns to provide constraints on ship NO_x emissions, and explicitly account for sensitivities to changing emissions in the model and satellite retrieval. The (non-linear) sensitivity of simulated NO_2 columns to changing NO_x emissions (the so-called β factor) found in this study is in the range 0.3–0.9, indicating that emission changes lead to substantial changes in NO_2 columns over ship lanes. We also account for the (non-linear) sensitivity of satellite observations to changing a priori NO_2 profiles. Although the effect of this sensitivity might be minor for small emission changes, the effect on observed NO_2 columns can be significant for large changes in NO_x emissions (up to 87 % of GEOS-Chem column change). Our findings stress the need for consistent information in the satellite retrieval and the model, as satellite derived vertical columns are never fully independent of model information (i.e. vertical NO_2 profiles).

Emissions in the main ship track of the Mediterranean Sea in our top-down inventory (0.13 Tg N) closely match the emissions strength of the AMVER-ICOADS inventory (0.12 Tg N) for 2005, and emissions in the Bay of Biscay and the North Sea appear more coherent with emissions in surrounding seas. Our results indicate that Mediterranean Sea emissions in the EMEP inventory are too high (by 60 %), which could have important consequences for local air quality simulations. Future work could focus on the effect of these reduced and relocated emissions on air quality. In the

North Sea ship track, our total top-down emissions amount to 0.05 Tg N for 2005 (35 % lower than EMEP). OMI top-down emissions for the Baltic Sea and the Bay of Biscay ship tracks are 0.05 Tg N (131 % higher than EMEP) and 0.08 Tg N (128 % higher than EMEP) for 2005, respectively. Our top-down emission inventory (0.96 Tg N for 2005, 1.0 Tg N for 2006) is about 11–15 % lower than the (regional) EMEP ship emission inventory (1.1 Tg N), and in closer agreement with the AMVER-ICOADS global emission inventory (0.8 Tg N).

Our study provides a framework for future studies to constrain ship NO_x emissions using satellite NO_2 observations. This may be particularly valuable given the paucity of measurements of ship pollution over open waters and the upcoming emission control measures. Future work will focus on expanding the analysis to more years, providing an OMI-constrained top-down ship NO_x emissions inventory for use in CTMs. Including observations of additional satellite instruments could also be explored in the future in order to reduce systematic and random errors in the top-down emissions.

Supplementary material related to this article is available online at http://www.atmos-chem-phys.net/14/1353/2014/acp-14-1353-2014-supplement.pdf.

Acknowledgements. This research was funded by the Netherlands Organisation for Scientific Research, NWO Vidi grant 864.09.001. We acknowledge the free use of tropospheric NO_2 column data from the OMI obtained from www.temis.nl.

Edited by: M. Van Roozendael

References

Acarreta, J. R., De Haan, J. F., and Stammes, P.: Cloud pressure retrieval using the O_2–O_2 absorption band at 477 nm, J. Geophys. Res.-Atmos., 109, D05204, doi:10.1029/2003JD003915, 2004.

Baughcum, S. L., Henderson, S. C., Tritz, T. G., and Pickett, D. C.: Scheduled Civil Aircraft Emission Inventories for 1992: Database Development and Analysis. NASA-CR-4700, National Aeronautics and Space Administration, Langley Research Center, Hampton, VA, USA, 1996.

Barkley, M. P., Kurosu, T. P., Chance, K., De Smedt, I., Van Roozendael, M., Arneth, A., Hagberg, D., and Guenther, A.: Assessing sources of uncertainty in formaldehyde air mass factors over tropical South America: Implications for top-down isoprene emission estimates, J. Geophys. Res.-Atmos., 117, D13304, doi:10.1029/2011JD016827, 2012.

Beirle, S., Platt, U., von Glasow, R., Wenig, M., and Wagner, T.: Estimate of nitrogen oxide emissions from shipping by satellite remote sensing, Geophys. Res. Lett., 31, L18102, doi:10.1029/2004GL020312, 2004.

Bertram, T. H., Thornton, J. A., Riedel, T. P., Middlebrook, A. M., Bahreini, R., Bates, T. S., Quinn, P. K., and Coffman, D. J.: Direct observations of N_2O_5 reactivity on ambient aerosol particles, Geophys. Res. Lett., 36, L19803, doi:10.1029/2009GL040248, 2009.

Boersma, K. F., Eskes, H. J., and Brinksma, E. J.: Error analysis for tropospheric NO_2 retrieval from space, J. Geophys. Res., 109, D04311, doi:10.1029/2003JD003962, 2004.

Boersma, K. F., Eskes, H. J., Meijer, E. W., and Kelder, H. M.: Estimates of lightning NO_x production from GOME satellite observations, Atmos. Chem. Phys., 5, 2311–2331, doi:10.5194/acp-5-2311-2005, 2005.

Boersma, K. F., Eskes, H. J., Veefkind, J. P., Brinksma, E. J., van der A, R. J., Sneep, M., van den Oord, G. H. J., Levelt, P. F., Stammes, P., Gleason, J. F., and Bucsela, E. J.: Near-real time retrieval of tropospheric NO_2 from OMI, Atmos. Chem. Phys., 7, 2103–2118, doi:10.5194/acp-7-2103-2007, 2007.

Boersma, K. F., Eskes, H. J., Dirksen, R. J., van der A, R. J., Veefkind, J. P., Stammes, P., Huijnen, V., Kleipool, Q. L., Sneep, M., Claas, J., Leitão, J., Richter, A., Zhou, Y., and Brunner, D.: An improved tropospheric NO_2 column retrieval algorithm for the Ozone Monitoring Instrument, Atmos. Meas. Tech., 4, 1905–1928, doi:10.5194/amt-4-1905-2011, 2011.

Brown, S. S., Dub, W. P., Fuchs, H., Ryerson, T. B., Wollny, A. G., Brock, C. A., Bahreini, R., Middlebrook, A. M., Neuman, J. A., Atlas, E., Roberts, J. M., Osthoff, H. D., Trainer, M., Fehsenfeld, F. C., and Ravishankara, A. R.: Reactive uptake coefficients for N_2O_5 determined from aircraft measurements during the Second Texas Air Quality Study: comparison to current model parameterizations, J. Geophys. Res.-Atmos., 114, D00F10, doi:10.1029/2008JD011679, 2009.

Butkovskaya, N., Kukui, A., and Le Bras, G.: HNO_3 forming channel of the $HO_2 + NO$ reaction as a function of pressure and temperature in the ranges of 72–600 torr and 223–323 K, J. Phys. Chem. A, 111, 9047–9053, doi:10.1021/jp074117m, 2007.

Butkovskaya, N., Rayez, M.-T., Rayez, J.-C., Kukui, A., and Le Bras, G.: Water vapor effect on the HNO_3 yield in the $HO_2 + NO$ reaction: experimental and theoretical evidence, J. Phys. Chem. A, 113, 11327–11342, doi:10.1021/jp811428p, 2009.

Chen, D., Wang, Y., McElroy, M. B., He, K., Yantosca, R. M., and Le Sager, P.: Regional CO pollution and export in China simulated by the high-resolution nested-grid GEOS-Chem model, Atmos. Chem. Phys., 9, 3825–3839, doi:10.5194/acp-9-3825-2009, 2009.

Corbett, J. J., Winebrake, J. J., Green, E. H., Kasibhatla, P., Eyring, V., and Lauer, A.: Mortality from ship emissions: a global assessment, Environ. Sci. Technol., 41, 8512–8518, 2007.

Davis, D. D., Grodzinsky, G., Kasibhatla, P., Crawford, J., Chen, G., Liu, S., Bandy, A., Thornton, D., Guan, H., and Sandholm, S.: Impact of ship emissions on marine boundary layer NO_x and SO_2 distributions over the Pacific Basin, Geophys. Res. Lett., 28, 235–238, 2001.

de Ruyter de Wildt, M., Eskes, H. J., and Boersma, K. F.: The global economic cycle and satellite-derived NO_2 trends over shipping lanes, Geophys. Res. Lett., 39, L01802, doi:10.1029/2011GL049541, 2012.

Denier van der Gon, H., Visschedijk, A., van Gijlswijk, R., and Kuenen, J.: High Resolution European Emission Inventory for the Years 2003–2007, TNO report TNO-060-UT-2011-0058: 49, Utrecht, 2011.

Dentener, F., van Weele, M., Krol, M., Houweling, S., and van Velthoven, P.: Trends and inter-annual variability of methane

emissions derived from 1979–1993 global CTM simulations, Atmos. Chem. Phys., 3, 73–88, doi:10.5194/acp-3-73-2003, 2003.

Eyring, V., Köhler, H. W., van Aardenne, J., and Lauer, A.: Emissions from international shipping: 1. The last 50 years, J. Geophys. Res., 110, D17305, doi:10.1029/2004JD005619, 2005.

Eyring, V., Isaksen, I. S. A., Berntsen, T., Collins, W. J., Corbett, J. J., Endresen, O., Grainger, R. G., Moldanova, J., Schlager, H., and Stevenson, D. S.: Transport impacts on atmosphere and climate: shipping, Atmos. Environ., 44, 4735–4771, 2010.

Franke, K., Richter, A., Bovensmann, H., Eyring, V., Jöckel, P., Hoor, P., and Burrows, J. P.: Ship emitted NO_2 in the Indian Ocean: comparison of model results with satellite data, Atmos. Chem. Phys., 9, 7289–7301, doi:10.5194/acp-9-7289-2009, 2009.

Hains, J. C., Boersma, K. F., Kroon, M., Dirksen, R. J., Cohen, R. C., Perring, A. E., Bucsela, E., Volten, H., Swart, D. P. J., Richter, A., Wittrock, F., Schoenhardt, A., Wagner, T., Ibrahim, O. W., van Roozendael, M., Pinardi, G., Gleason, J. F., Veefkind, J. P., and Levelt, P.: Testing and improving OMI DOMINO tropospheric NO_2 using observations from the DANDELIONS and INTEX-B validation campaigns, J. Geophys. Res., 115, D05301, doi:10.1029/2009JD012399, 2010.

Henderson, B. H., Pinder, R. W., Crooks, J., Cohen, R. C., Carlton, A. G., Pye, H. O. T., and Vizuete, W.: Combining Bayesian methods and aircraft observations to constrain the $HO\bullet+NO_2$ reaction rate, Atmos. Chem. Phys., 12, 653–667, doi:10.5194/acp-12-653-2012, 2012.

Huijnen, V., Eskes, H. J., Poupkou, A., Elbern, H., Boersma, K. F., Foret, G., Sofiev, M., Valdebenito, A., Flemming, J., Stein, O., Gross, A., Robertson, L., D'Isidoro, M., Kioutsioukis, I., Friese, E., Amstrup, B., Bergstrom, R., Strunk, A., Vira, J., Zyryanov, D., Maurizi, A., Melas, D., Peuch, V.-H., and Zerefos, C.: Comparison of OMI NO2 tropospheric columns with an ensemble of global and European regional air quality models, Atmos. Chem. Phys., 10, 3273–3296, doi::10.5194/acp-10-3273-2010, 2010.

IMO: Revised Marpol Annex VI, Regulation for the prevention of air pollution from ships and NO_x technical code 2008, 2009 Edn., Tech. rep., IMO publishing, London, ISBN 978-92-801-4243-3, 2009.

IPCC: Climate Change 2007: Impacts, Adaptation and Vulnerability, Contribution of Working Group II to the Fourth Assessment Report of the Intergovernmental Panel on Climate Change, edited by: Parry, M. L., Canziani, O. F., Palutikof, J. P., van der Linden, P. J., and Hanson, C. E., Cambridge University Press, Cambridge, UK, 976 pp., 2007.

Irie, H., Boersma, K. F., Kanaya, Y., Takashima, H., Pan, X., and Wang, Z. F.: Quantitative bias estimates for tropospheric NO_2 columns retrieved from SCIAMACHY, OMI, and GOME-2 using a common standard for East Asia, Atmos. Meas. Tech., 5, 2403–2411, doi:10.5194/amt-5-2403-2012, 2012.

Jaeglé, L., Steinberger, L., Martin, R. V., and Chance, K.: Global partitioning of NO_x sources using satellite observations: relative roles of fossil fuel combustion, biomass burning and soil emissions, Faraday Discuss., 130, 407–423, doi:10.1039/b502128f, 2005.

Jalkanen, J.-P., Brink, A., Kalli, J., Pettersson, H., Kukkonen, J., and Stipa, T.: A modelling system for the exhaust emissions of marine traffic and its application in the Baltic Sea area, Atmos. Chem. Phys., 9, 9209–9223, doi:10.5194/acp-9-9209-2009, 2009.

Kasibhatla, P., Levy II, H., Moxim, W. J., Pandis, S. N., Corbett, J. J., Peterson, M. C., Honrath, R. E., Frost, G. J., Knapp, K., Parrish, D. D., and Ryerson, T. B.: Do emissions from ships have a significant impact on concentrations of nitrogen oxides in the marine boundary layer?, Geophys. Res. Lett., 27, 2229–2232, 2000.

Kleipool, Q. L., Dobber, M. R., de Haan, J. F., and Levelt, P. F.: Earth surface reflectance climatology from 3 years of OMI data, J. Geophys. Res.-Atmos., 113, D18308, doi:10.1029/2008JD010290, 2008.

Lamsal, L. N., Martin, R. V., Padmanabhan, A., van Donkelaar, A., Zhang, Q., Sioris, C. E., Chance, K., Kurosu, T. P., and Newchurch, M. J.: Application of satellite observations for timely updates to global anthropogenic NO_x emission inventories, Geophys. Res. Lett., 38, L05810, doi:10.1029/2010GL046476, 2011.

Lauer, A., Eyring, V., Hendricks, J., Jöckel, P., and Lohmann, U.: Global model simulations of the impact of ocean-going ships on aerosols, clouds, and the radiation budget, Atmos. Chem. Phys., 7, 5061–5079, doi:10.5194/acp-7-5061-2007, 2007.

Lawrence, M. G. and Crutzen, P. J.: Influence of NO_x emissions from ships on tropospheric photochemistry and climate, Nature, 402, 167–170, 1999.

Levelt, P. F., van den Oord en M. R. Dobber, G. H. J., Mälkki, A., Visser, H., de Vries, J., Stammes, P., Lundell, J. O. V., and Saari, H.: The Ozone Monitoring Instrument, IEEE T. Geosci. Remote, 44, 1093–1109, doi:10.1109/TGRS.2006.872333, 2006.

Lin, J.-T., Liu, Z., Zhang, Q., Liu, H., Mao, J., and Zhuang, G.: Modeling uncertainties for tropospheric nitrogen dioxide columns affecting satellite-based inverse modeling of nitrogen oxides emissions, Atmos. Chem. Phys., 12, 12255–12275, doi:10.5194/acp-12-12255-2012, 2012.

Lu, Z. and Streets, D. G.: Increase in NO_x emissions from indian thermal power plants during 1996–2010: unit-based inventories and multisatellite observations, Environ. Sci. Technol., 46, 7463–7470, doi:10.1021/es300831w, 2012.

Macintyre, H. L. and Evans, M. J.: Sensitivity of a global model to the uptake of N_2O_5 by tropospheric aerosol, Atmos. Chem. Phys., 10, 7409–7414, doi:10.5194/acp-10-7409-2010, 2010.

Mao, J., Jacob, D. J., Evans, M. J., Olson, J. R., Ren, X., Brune, W. H., Clair, J. M. St., Crounse, J. D., Spencer, K. M., Beaver, M. R., Wennberg, P. O., Cubison, M. J., Jimenez, J. L., Fried, A., Weibring, P., Walega, J. G., Hall, S. R., Weinheimer, A. J., Cohen, R. C., Chen, G., Crawford, J. H., McNaughton, C., Clarke, A. D., Jaeglé, L., Fisher, J. A., Yantosca, R. M., Le Sager, P., and Carouge, C.: Chemistry of hydrogen oxide radicals (HO_x) in the Arctic troposphere in spring, Atmos. Chem. Phys., 10, 5823–5838, doi:10.5194/acp-10-5823-2010, 2010.

Marmer, E., Dentener, F., Aardenne, J. v., Cavalli, F., Vignati, E., Velchev, K., Hjorth, J., Boersma, F., Vinken, G., Mihalopoulos, N., and Raes, F.: What can we learn about ship emission inventories from measurements of air pollutants over the Mediterranean Sea?, Atmos. Chem. Phys., 9, 6815–6831, doi:10.5194/acp-9-6815-2009, 2009.

Martin, R. V., Jacob, D. J., Chance, K., Kurosu, T. P., Palmer, P. I., and Evans, M. J.: Global inventory of nitrogen oxide emissions constrained by space-based observations of NO_2 columns, J. Geophys. Res., 108, 4537, doi:10.1029/2003JD003453, 2003.

Martin, R. V., Sioris, C. E., Chance, K., Ryerson, T. B., Bertram, T. H., Woolbridge, P. J., Cohen, R. C., Neuman, J. A., Swanson, A., and Flocke, F. M.: Evaluation of space-based constraints on global nitrogen oxide emissions with regional aircraft measurements over and downwind of Eastern North America, J. Geophys. Res., 111, D15308, doi:10.1029/2005JD006680, 2006.

Mollner, A. K., Valluvadasan, S., Feng, L., Sprague, M. K., Okumura, M., Milligan, D. B., Bloss, W. J., Sander, S. P., Martien, P. T., Harley, R. A., McCoy, A. B., and Carter, W. P. L.: Rate of gas phase association of hydroxyl radical and nitrogen dioxide, Science, 330, 646–649, doi:10.1126/science.1193030, 2010.

Olivier, J., Peters, J., Granier, C., Pétron, G., Müller, J. F., and Wallens, S.: Present and future surface emissions of atmospheric compounds, POET Report #2, EU project EVK2- 1999-00011, 2003.

Olivier, J. G. J. and Berdowski, J. J. M.: Global emissions sources and sinks, in: The Climate System, Lisse, the Netherlands, 33–78 pp., 2001.

Paoli, R., Cariolle, D., and Sausen, R.: Review of effective emissions modeling and computation, Geosci. Model Dev., 4, 643–667, doi:10.5194/gmd-4-643-2011, 2011.

Paxian, A., Eyring, V., Beert, W., Sausen, R., and Wright, C.: Present-day and future global bottom-up ship emissions inventories including polar routes, Environ. Sci. Technol., 44, 1333–1339, 2010.

Richter, A., Eyring, V., Burrows, J. P., Bovensmann, H., Lauer, A., Sierk, B., and Crutzen, P. J.: Satellite measurements of NO_2 from international shipping emissions, Geophys. Res. Lett., 31, L23110, doi:10.1029/2004GL020822, 2004.

Sauvage, B., Martin, R. V., van Donkelaar, A., and Ziemke, J. R.: Quantification of the factors controlling tropical tropospheric ozone and the South Atlantic maximum, J. Geophys. Res., 112, D11309, doi:10.1029/2006JD008008, 2007.

Schreier, M., Mannstein, H., Eyring, V., and Bovensmann, H.: Global ship track distribution and radiative forcing from 1 year of AATSR data, Geophys. Res. Lett., 34, L17814, doi:10.1029/2007GL030664, 2007.

Sneep, M., de Haan, J. F., Stammes, P., Wang, P., Vanbauce, C., Joiner, J., Vasilkov, A. P., and Levelt, P. F.: Three-way comparison between OMI and PARASOL cloud pressure products, J. Geophys. Res.-Atmos., 113, D15S23, doi:10.1029/2007JD008694, 2008.

Stavrakou, T., Müller, J.-F., Boersma, K. F., van der A, R. J., Kurokawa, J., Ohara, T., and Zhang, Q.: Key chemical NO_x sink uncertainties and how they influence top-down emissions of nitrogen oxides, Atmos. Chem. Phys., 13, 9057–9082, doi:10.5194/acp-13-9057-2013, 2013.

Valin, L. C., Russell, A. R., Hudman, R. C., and Cohen, R. C.: Effects of model resolution on the interpretation of satellite NO_2 observations, Atmos. Chem. Phys., 11, 11647–11655, doi:10.5194/acp-11-11647-2011, 2011.

van der Werf, G. R., Randerson, J. T., Giglio, L., Collatz, G. J., Kasibhatla, P. S., and Arellano Jr., A. F.: Interannual variability in global biomass burning emissions from 1997 to 2004, Atmos. Chem. Phys., 6, 3423–3441, doi:10.5194/acp-6-3423-2006, 2006.

Vestreng, V.: Review and Revision, Emission data reported to CLRTAP, MSC-W Status Report 2003, Tech. rep., The Norwegian Meteorological Institute, Oslo, Norway, 2003.

Vestreng, V., Mareckova, K., Kakareka, S., Malchykhina, A., and Kukharchyk, T.: Inventory Review 2007; Emission Data Reported to LRTAP Convention and NEC Directive, MSC-W Technical Report 1/07, Tech. rep., The Norwegian Meteorological Institute, Oslo, Norway, 2007.

Vinken, G. C. M., Boersma, K. F., Jacob, D. J., and Meijer, E. W.: Accounting for non-linear chemistry of ship plumes in the GEOS-Chem global chemistry transport model, Atmos. Chem. Phys., 11, 11707–11722, doi:10.5194/acp-11-11707-2011, 2011.

Wang, C., Corbett, J. J., and Firestone, J.: Improving spatial representation of global ship emissions inventories, Environ. Sci. Technol., 42, 193–199, 2008.

Wang, S. W., Zhang, Q., Streets, D. G., He, K. B., Martin, R. V., Lamsal, L. N., Chen, D., Lei, Y., and Lu, Z.: Growth in NO_x emissions from power plants in China: bottom-up estimates and satellite observations, Atmos. Chem. Phys., 12, 4429–4447, doi:10.5194/acp-12-4429-2012, 2012.

Wang, X. Y., McElroy, M. B., Jacob, D. J., and Yantosca, R. M.: A nested grid formulation for chemical transport over Asia: applications to CO, J. Geophys. Res., 109, D22307, doi:10.1029/2004JD005237, 2004.

Wang, Y., Jacob, D. J., and Logan, J.: Global simulation of tropospheric O_3–NO_x–hydrocarbon chemistry, 1. Model formulation, J. Geophys. Res., 130, 10713–10726, 1998.

Yevich, R. and Logan, J. A.: An assessment of biofuel use and burning of agricultural waste in the developing world, Global Biogeochem. Cy., 17, 1095, doi:10.1029/2002GB001952, 2003.

Yienger, J. J., and Levy II, H.: Empirical model of global soil-biogenic NO_x emissions, J. Geophys. Res., 100, 11447–11464, 1995.

Zhang, L., Jacob, D. J., Knipping, E. M., Kumar, N., Munger, J. W., Carouge, C. C., van Donkelaar, A., Wang, Y. X., and Chen, D.: Nitrogen deposition to the United States: distribution, sources, and processes, Atmos. Chem. Phys., 12, 4539–4554, doi:10.5194/acp-12-4539-2012, 2012.